Lawrence Berkeley National Laboratory

LBL Publications

Title

A Uranyl Peroxide Dimer in the Gas Phase

Permalink

https://escholarship.org/uc/item/7vv6v60m

Journal

Inorganic Chemistry, 56(7)

ISSN

0020-1669

Authors

Dau, Phuong D

Dau, Phuong V

Rao, Linfeng

et al.

Publication Date

2017-04-03

DOI

10.1021/acs.inorgchem.7b00187

Copyright Information

This work is made available under the terms of a Creative Commons Attribution-NonCommercial-NoDerivatives License, available at https://creativecommons.org/licenses/by-nc-nd/4.0/

Peer reviewed

eScholarship.org Powered by the California Digital Library
University of California

A Uranyl Peroxide Dimer in the Gas Phase

Phuong D. Dau[1], Phuong V. Dau[1], Linfeng Rao[1], Attila Kovács[*,2], John K. Gibson[*,1]

[1]Chemical Sciences Division, Lawrence Berkeley National Laboratory, Berkeley, California, 94720, United States

[2]European Commission, Joint Research Centre, Institute for Transuranium Elements, P.O. Box 2340, 76125 Karlsruhe, Germany

[*]Corresponding authors: Attila.KOVACS@ec.europa.eu; JKGibson@lbl.gov

Abstract

The gas-phase uranyl peroxide dimer, $[(UO_2)_2(O_2)(L)_2]^{2+}$ where L = 2,2'-trifluoroethylazanediyl)bis(N,N'-dimethylacetamide), was synthesized by electrospray ionization of a solution of UO_2^{2+} and L. Collision induced dissociation of this dimer resulted in endothermic O-atom elimination to give $[(UO_2)_2(O)(L)_2]^{2+}$, which was found to spontaneously react with water via exothermic hydrolytic chemisorption to yield $[(UO_2)_2(OH)_2(L)_2]^{2+}$. Density functional theory computations of the energies for the gas-phase reactions are in accord with observations. The structures of the observed uranyl dimer were computed, with that of the peroxide of particular interest as a basis to evaluate the formation of condensed phase uranyl peroxides with bent structures. The computed dihedral angle in $[(UO_2)_2(O_2)(L)_2]^{2+}$ is 145^o, indicating a substantial deviation from the planar structure with a dihedral angle of 180^o. Energies needed to induce bending in the most elementary gas-phase uranyl peroxide complex, $[(UO_2)_2(O_2)]^{2+}$, were computed. It was found that bending from the lowest-energy planar structure to dihedral angles up to 140^o required energies of <10 kJ/mol. The gas-phase results demonstrate the inherent stability of the uranyl peroxide moiety, and support the notion that the uranyl-peroxide-uranyl structural unit is intrinsically planar with only minor energy perturbations needed to form the bent structures found in studtite and uranyl peroxide nanostructures.

Introduction

The peroxide moiety, O_2^{2-}, is unusual in naturally occurring minerals. In 2003, Burns and Hughes reported the structure of studtite, $[(UO_2)(O_2)(H_2O)_2](H_2O)_2$, which consists of one-dimensional chains with uranyl moieties, UO_2^{2+}, linked by peroxides.[1] A fascinating feature of the studtite structure is that the uranyl-peroxide-uranyl dihedral angles—i.e., the angles between the two planes defined by adjacent uranyl-peroxide moieties (see Fig. 9)—is 140°, which is far from the 180° planar orientation that might be expected based on elementary steric repulsion considerations. This highly bent structural motif suggested the possibility of creating cage-like nanostructures based on uranyl-peroxide-uranyl building blocks. The first "uranyl peroxide nanospheres" resulting from this hypothesis, reported by Burns et al. in 2005, were composed of 24, 28 and 32 uranyl peroxide building blocks that form closed cage structures.[2] Since then, Burns and co-workers have synthesized and characterized many nanoscale uranyl peroxide cage and other clusters that incorporate the bent uranyl peroxide structural unit.[3-8] Among these clusters is one that comprises 60 uranyl moieties and bears a remarkable resemblance to the prototypical nanostructure buckminsterfullerene, C_{60}.[9] Uranium oxide nanostructure materials are of interest for potential relevance to advanced nuclear technology, including processing[10] and degradation[11] of nuclear fuels.

There is fundamental interest in understanding the driving forces for the formation of the bent uranyl peroxide cage nanostructures, and the nature of the bonding in them. Several computational studies have been performed, with an emphasis on understanding the origins of the bent nature of the uranyl-peroxide-uranyl building block that enables the curvature necessary to produce closed-cage nanospheres and other distinctive materials.[12-20] The cations employed to achieve charge neutrality in peroxide-rich clusters were found to have a substantial effect on the extent of deviation from a 180° dihedral angle.[12-14,19] Qiu et al.[18] concluded that the $[UO_2^{2+}\text{-}(O_2^{2-})\text{-}UO_2^{2+}]$ moiety is not rigid and that deviations from a planar geometry can be induced with minor energy expenditure. The most elementary uranyl peroxide structures, dimers comprising two uranyl moieties and a single bridging peroxide, have been reported in the condensed phase.[21,22] In addition to dimers, condensed phase uranyl peroxide monomers[23] and trimers[24] have been reported. Uranyl peroxide has also been found in the ternary carbonate complex $UO_2(O_2)(CO_3)_2^{4-}$.[25] The goal of the present work was to approach the topic of uranyl peroxides from an extremely fundamental perspective in gas-phase dimeric species, by both experiment and theory. A key attribute of relatively small gas-phase species in the absence of perturbations introduced by solvent or extended coordination in solids is that they are amenable to particularly accurate computational evaluation and can elucidate fundamental aspects of structure and bonding in metal complexes.[26,27] The goal of the present work is to extend understanding of uranyl peroxides by studying gas-phase dimers. Several diamide amine-functionalized ligands have been synthesized to study the solution thermodynamics complexation with lanthanide ions.[28] The generic structure of these ligands is shown in Figure 1. It has been demonstrated that such strongly coordinating multidentate ligands can stabilize multiply charged metal cations, including UO_2^{2+}, from solution to gas during electrospray ionization (ESI).[29,30] In the present work, 2,2'-trifluoroethylazanediyl)bis(N,N'-dimethylacetamide) (TFABDMA; Scheme 1)

was employed to synthesize a gas-phase uranyl peroxide dimer with a 2+ charge. The chemical properties of this dimer studied experimentally are in good agreement with predictions from density functional theory (DFT) computations. DFT was furthermore employed to better understand at a fundamental level the origins of bent uranyl peroxide structures.

Experimental Details

Ligand Synthesis

Starting materials and solvents were purchased and used without further purification from commercial suppliers (Sigma-Aldrich, Alfa Aesar, EMD, TCI, Cambridge Isotope Laboratories, Inc., and others). 5-Methyl-2-(*p*-tolyl)pyridine (model C,N-ligand) was synthesized as described.[31] Proton nuclear magnetic resonance spectra (^{1}H NMR) were recorded on a Bruker FT-NMR spectrometer (300 MHz for ^{1}H). Chemical shifts were quoted in parts per million (ppm) referenced to the appropriate solvent peak or 0 ppm for TMS. The following abbreviations were used to describe peak patterns when appropriate: s = singlet, q = quartet. Coupling constants, *J*, are reported in Hertz unit (Hz).

The TFABDMA ligand was synthesized as summarized in Scheme 1, in a manner analogous to that employed for other diamide amine-functionalized ligands.[28] Specifically, 2,2,2-Trifluoroethylamine (5.1 mmol, 0.4 mL), 2-chloro-*N*-dimethylacetamide (10.5 mmol, 1.1 mL), K_2CO_3 (31 mmol, 4.2 g), and KI (6.0 mmol, 1.0 g) were added in a round-bottom flask. The mixture was stirred, and heated to reflux in CH_3CN (100 mL) for 2 days. K_2CO_3 and KI were filtered off, and CH_3CN was removed under vacuum to yield a yellow liquid. The yellow liquid was brought up with about 50 mL water and 150 mL chloroform. The mixture was stirred for about 1 h. The organic layer was separated and dried under vacuum to yield a yellow liquid as the product (29.4 % yield). ^{1}H NMR spectra ($CDCl_3$, 300 MHz, ppm): δ 3.721 (s, 4H); δ 3.427 (q, 2H); δ 2.965 (s, 6H); δ 2.914 (s, 6H).

Gas-Phase Experiments

The general gas-phase experimental approach has been described previously.[32] The di-cationic uranyl dimer with a bridging peroxide and supported by two TFABDMA ligands, was produced by ESI of an ethanol solution (~1% H_2O) containing 0.1 mM UO_2^{2+} and 0.1 mM TFABDMA. The UO_2^{2+} reagent was from a stock aqueous solution of 10 mM $UO_2(ClO_4)_2$ (pH = 2). *The ^{238}U used in this work is radioactive and must be handled with proper controls.*[33] The experiments were performed using an Agilent 6340 quadrupole ion trap tandem mass spectrometer with MS^n collision induced dissociation (CID) fragmentation capability. Ions in the trap can furthermore undergo ion-molecule reactions at ~300 K [34] by applying a reaction time of up to 10 s. Anion mass spectra were acquired using the following parameters: solution flow rate, 60 µL/h; nebulizer gas pressure, 6 psi; capillary voltage offset and current, -3200 V and 6.1 nA; end plate voltage offset and current, -500 V and 100 nA ; dry gas flow rate, 2 l/min; dry gas temperature, 325 °C; capillary exit, 142 V; skimmer, 26 V; octopole 1 and 2 DC, 13.8 V and 3.1 V; octopole RF amplitude, 58 Vpp; lens 1 and 2, -4.8 V and -65 V; trap drive, 217. Nitrogen gas for nebulization and drying was supplied from the boil-off of a liquid nitrogen Dewar. The background water pressure in the ion trap is estimated as ~10^{-6} Torr;[35] reproducibility of hydration rates of $UO_2(OH)^+$ [35] established that

the water pressure was constant to within 10%. The helium buffer gas pressure in the trap is constant at ~10^{-4} Torr.

Computational Details

The computations were performed with the Gaussian09 suite of programs,[36] using the B3LYP exchange-correlation functional.[37,38] Preliminary calculations on the conformational space of all three target molecules were carried out with the 6-31+G** basis set. For U the Stuttgart-Cologne small-core pseudopotential (ECP60MWB[39]) was used in conjunction with a 14s13p10d8f6g valence basis set contracted to 10s9p5d4f3g (ECP60MWB_SEG[40]). All complexes for which computations were performed have a net charge of 2+ and singlet spin multiplicity. According to test calculations the triplet-states are considerably higher (around 200 kJ/mol) in energy than the singlets. The minimum character of the obtained stationary points on the potential energy surface was confirmed in all cases by frequency analysis.

Calculations at a higher level of theory were performed only for the lowest-energy conformers. This higher level included the extension of B3LYP with the D3 version of Grimme's dispersion correction using the original D3 damping function,[41] the cc-pVTZ and aug-cc-pVTZ basis sets[42] for C, H and N, O, F, respectively, as well as the UltraFine integration grid (99 radial shells and 590 angular points per shell). The study of the bonding properties was based on natural bond orbital (NBO) analysis[43] providing atomic charges and Wiberg bond indices,[44] this latter property giving information on the covalent bond order. The NBO analysis was performed by means of the NBO5.9 code[45] coupled with Gaussian09. The thermodynamic data were obtained using the rigid rotor harmonic oscillator approximation. Because of the closed-shell character of the studied complexes the electronic contribution could be neglected.

Results and Discussion

The synthesis and reactivity experimental studies of the $[(UO_2)_2(O_2)(L)_2]^{2+}$ dimer and reaction products are described. The computed structures, bonding and reaction energies are then presented; comparison of relevant computed properties is made with the experimental observations. Computational results on a further simplified model gas-phase complex are employed to further evaluate the nature of bending in uranyl peroxides.

Synthesis and Reactivity of Gas-Phase Uranyl Dimer Cation Complexes

The ESI mass spectrum of the uranyl/L (L = TFABDMA) solution is shown in Figure 2. The dominant species are monopositive bare and ligated uranyl(V), as is typical for ESI of solutions of dipositive uranyl(VI) using the ESI-QIT/MS employed in this work.[35] Although it has been possible to produced dipositive uranyl complexes using this instrument, the yields have been low and a stronger coordinating Lewis base than water was necessary to stabilize the higher charge-state.[33] The relatively harsh conditions imposed by this particular instrument contrasts with other ESI experiments in which dipositive and tripositive hydrated metal ion complexes have been generated and studied.[46,47] Also apparent in Fig. 2 is a peak due to a complex of Na^+, which is a notoriously ubiquitous metal ion contaminant in solutions. The dipositive species of particular interest in the present study, identified in Fig.

2b, is $[(UO_2)_2(O_2)(L)_2]^{2+}$, which is formally the uranyl peroxide dimer $[(UO_2^{2+})_2(O_2^{2-})(L)_2]^{2+}$. This composition and charge state is confirmed by m/z peak separation of 0.5 (i.e., z = 2), and by the CID mass spectrum in Fig. 3a, where charge-separation to give the expected monopositive fragments is apparent. An elementary hypothetical reaction that would yield the observed dimer is given by equation (1).

$$2(UO_2)^+ + O_2 + 2(L) \rightarrow [(UO_2)_2(O_2)(L)_2]^{2+} \qquad (1)$$

This simple reaction is not established by the results and it is not known at what stage of the complex ESI process such a hypothetical association reaction might occur, or if the dimeric species is already present in solution. It was not possible to substantially enhance the yield of the peroxide dimer by adjusting the ESI and ion transport conditions to resolve the origins of the gas-phase complex. The solubility of O_2 in ethanol at room temperature and atmospheric pressure (0.2 bar O_2) is ca. 0.1 mM,[48] which is comparable to the concentration of uranyl and L; if the product of equation (1) is sufficiently stable there should thus be adequate O_2 in solution to account for the observed abundance of the uranyl(VI) dimeric complex, which is lower than that of bare and ligated uranyl(V). A notable aspect of the observation of a uranyl peroxide dimer under these conditions is that peroxide was not added to the solution, as is typically necessary for formation of uranyl peroxides. In the case of the mineral studtite, the bridging peroxide moieties are considered to derive from peroxide formation as a result of alpha-radiolysis of water by uranium.[1] Hypothetical reaction (1) assumes reduction of UO_2^{2+} in solution to UO_2^+ during ESI, which is a well-established phenomenon and is evidenced by the dominant UO_2^+ peak in Figure 2a. This reduction is consistent with metal ion reduction that is more generally known to occur during ESI.[49] Reaction (1) corresponds to oxidation of UO_2^+ to UO_2^{2+} concomitant with *formal* reduction of O_2 to O_2^{2-}. Although the studied mineral system is substantially more complex than the dimer considered here, it should be noted that the U(VI/V) reduction potential in studtite has been reported.[50] It has been demonstrated that in the gas phase O_2 is reduced to O_2^- by one UO_2^+ ion,[35] such that reduction of O_2 to O_2^{2-} by two UO_2^+ ions is a reasonable hypothesis. Another key aspect of reaction (1) is the retention of a dipositive charge in the peroxide complex—strongly binding electron donor polydentate ligands such as TFABDMA are known to stabilize multiply charged cations from solution to gas during ESI.[29] Also apparent in Fig. 2 is a peak due to $[(UO_2)_2(O)(L)_2]^{2+}$, which can result from fragmentation of $[(UO_2)_2(O_2)(L)_2]^{2+}$, as discussed below. Although peroxide was not deliberately added to the solution, potential sources include photolysis[51] and decomposition of perchlorate in solution.[52]

The CID fragmentation results for $[(UO_2)_2(O_2)(L)_2]^{2+}$ are shown in Figure 3a. The fragmentation pathways given by reactions (2) and (3) were observed.

$$[(UO_2)_2(O_2)(L)_2]^{2+} \rightarrow [UO_2(O_2)(L)]^+ + [UO_2(L)]^+ \qquad (2)\ [CID]$$

$$[(UO_2)_2(O_2)(L)_2]^{2+} \rightarrow [(UO_2)_2(O)(L)_2]^{2+} + O \qquad (3)\ [CID]$$

Because the highest accessible uranium oxidation state is U(VI), the two products of the CID charge separation reaction (2) are assigned as a uranyl(VI) superoxide[35] and a reduced uranyl(V) complex, respectively; the peroxide moiety, O_2^{2-}, is evidently oxidized to a superoxide, O_2^-, concomitant with reduction of U(VI) to U(V). The computed reactant and product structures and the energy for reaction (3) are discussed below; in essence, the

peroxide bridge (*formally* O_2^{2-}) is converted to an oxygen atom bridge (*formally* O^{2-}) to yield a dimer in which both uranyl moieties remain in the hexavalent oxidation state.

A CID mass spectrum for $[(UO_2)_2(O)(L)_2]^{2+}$ is shown in Figure 3b. The dominant product, $[(UO_2)_2(OH)_2(L)_2]^{2+}$, also results from the spontaneous reaction of the monoxide-bridged dimer with background water in the ion trap, as discussed below. As for CID reaction (2), the charge separation products apparent in Fig. 3b, $[UO_2(L)]^+$ and $[UO_2(F)(L)]^+$, are uranyl(V) and uranyl(VI) complexes, respectively. Retention of the U(VI) oxidation state is achieved by abstraction of a fluoride anion from the ligand, a phenomenon that has been previously observed and reflects the high affinity of uranium for fluorine.[53] In contrast to $[(UO_2)_2(O_2)(L)_2]^{2+}$, charge-separation into two monopositive fragments comprising all of the original constituents is not observed for $[(UO_2)_2(O)(L)_2]^{2+}$. The absence of $[UO_2(O)(L)]^+$ as a CID product can be attributed to the lower stability of the radical atomic oxygen ligand, O^-, compared with the superoxide ligand, O_2^-, in $[UO_2(O_2)(L)]^+$. The dominant product from CID of $[(UO_2)_2(O)(L)_2]^{2+}$ (Fig. 3b) is water-addition to yield $[(UO_2)_2(OH)_2(L)_2]^{2+}$, the structure of which was computed to be a bridging bis-hydroxide. This is not a fragmentation product but rather the result of chemisorption addition of H_2O to $[(UO_2)_2(O)(L)_2]^{2+}$ (see below). As is evident in Fig. 3c, CID of $[(UO_2)_2(OH)_2(L)_2]^{2+}$ results almost entirely in the reverse water-elimination process to yield $[(UO_2)_2(O)(L)_2]^{2+}$ and H_2O.

CID results in endothermic fragmentation, although exothermic reactions with background gases in the ion trap, including water-addition as is evident in Fig. 3b, can also occur during the CID timescale. In contrast, isolation of an ion followed by a reaction period reveals only spontaneous ion-molecule reactions with background gases, typically O_2 and/or H_2O, that are present in the ion trap. To fulfill the requirement for conservation of energy, reactions observed under non-CID conditions must have energy profiles that do not exceed the energy of the separated reactant ion and molecule; these reactions must be exothermic and present no barrier above the reactant asymptote energy. Reactivity results for $[(UO_2)_2(O_2)(L)_2]^{2+}$, $[(UO_2)_2(O)(L)_2]^{2+}$ and $[UO_2(L)]^+$ with reactive background gases in the ion trap are shown in Figure 4. Both of the latter species exhibit substantial reactivity with water for a reaction time of 50 ms, whereas the $[(UO_2)_2(O_2)(L)_2]^{2+}$ complex exhibits no reactivity under similar conditions even for a much longer reaction time of 1000 ms. The uranyl peroxide dimer is unreactive with both O_2 and H_2O, which is an indication of its intrinsic stability.

The results in Figure 4b and 4c reveal that $[(UO_2)_2(O)(L)_2]^{2+}$ and $[UO_2(L)]^+$ both spontaneously add water. For the latter, the process is assumed to be simple hydration, as is typical for coordinatively unsaturated uranyl cation complexes.[35] The monopositive U(V) complex also exhibits spontaneous addition of O_2 to yield $[UO_2(O_2)L]^+$, which in analogy with previous results,[35,54,55] is presumed to be a superoxide in which U(V) is oxidized to U(VI). As discussed below, spontaneous addition of water to $[(UO_2)_2(O)(L)_2]^{2+}$ occurs by chemisorption reaction (4).

$$[(UO_2)_2(O)(L)_2]^{2+} + H_2O \rightarrow [(UO_2)_2(OH)_2(L)_2]^{2+} \qquad (4)$$

As noted above and as is apparent in Fig. 3b, CID of $[(UO_2)_2(O)(L)_2]^{2+}$ yields primarily the product of reaction (4). The timeframe of CID is roughly 50 ms, in accord with the similar yields of $[(UO_2)_2(OH)_2(L)_2]^{2+}$ in Figures 3c and 4b; the somewhat greater yield in the former

CID mass spectrum may indicate enhancement of the rate for reaction (4) under hyperthermal conditions.

Computed Structures and Energetics: Comparison with Experiment

The first issue to address is the structures of the observed uranyl dimer complexes. The main interactions with the terminal neutral TFABDMA ligands are electrostatic and donor-acceptor, between UO_2^{2+} and the two oxo groups and the central tertiary amine group of the ligand. These interactions introduce constraints on the structure of the TFABDMA ligands, but due to rotation of the CF_3 group around the C-C bond and the flexibility of some torsional angles, a few conformers are possible. These conformers are very close in energy: within 4 kJ/mol for $[(UO_2)_2(O_2)(L)_2]^{2+}$ and $[(UO_2)_2(O)(L)_2]^{2+}$, and within 9 kJ/mol for $[(UO_2)_2(OH)_2(L)_2]^{2+}$. A result of these small differences in energies is that in the gas phase, particularly under the non-equilibrium conditions of the experiments reported here, a mixture of conformers is likely. However, the low-energy conformational changes are expected to have only marginal influence on the UO_2^{2+}-ligand interactions such that the properties of the global minima structures adequately characterize the complexes.

The optimized (global minimum) calculated structures of the three complex molecules are shown in Figure 5 (for clarity the ligand hydrogens are not shown). Selected structural parameters are given in Table 2; the Cartesian coordinates of the three global minimum structures are included as SI.

The calculated reaction enthalpies (ΔH^{298}) in Table 1 confirm that the formation of $[(UO_2)_2(O)(L)_2]^{2+}$ from $[(UO_2)_2(O_2)(L)_2]^{2+}$ by elimination of an O atom, reaction (3), is endothermic. This is in accord with the observation of this process under CID conditions (Fig. 3a), in competition with dissociation of the complex into two monopositive fragments according to reaction (2). In contrast, chemisorption hydrolysis reaction (4) is computed to be substantially exothermic; this is in accord with the experimental observation that it occurs spontaneously under thermal conditions. Whereas the peroxide dimer, $[(UO_2)_2(O_2)(L)_2]^{2+}$, is stable with respect to hydrolysis, $[(UO_2)_2(O)(L)_2]^{2+}$ hydrolytically adds water to yield $[(UO_2)_2(OH)_2(L)_2]^{2+}$ in which the single bridging O atom has been replaced by two bridging OH moieties.

The bonding in related model uranyl dimer complexes has been analyzed in two previous studies. Miró et al. computed the cationic $[UO_2]_2(\mu\text{-}\eta^2\text{:}\eta^2\text{-}O_2(H_2O)_6]^{2+}$ model and analyzed the deformation of four frontier molecular orbitals when the planar D_{2h} structure changed to a bent C_{2v} structure.[13] The energy advantage of bending was attributed to an increased orbital overlap between the uranium atoms and the peroxo bridge in the HOMO orbital and to decreased interactions between these moieties in HOMO-1. Vlaisavljevich et al.[12] studied the neutral $[(UO_2)_2(O_2)_5Na_6]$ and $[(UO_2)_2(O_2)_4(OH)_2Na_6]$ complexes. In the peroxide $[(UO_2)_2(O_2)_5Na_6]$ molecule, the O_2^{2-} moiety (where 2- is the *formal c*harge) forms a bridge between the two uranyls. The main bonding interaction corresponds to the overlap of a π orbital of O_2^{2-} with U 6p orbitals. This important role of U 6p orbitals was explained by substantial involvement of the valence U 6d and 5f orbitals in bonding with the uranyl oxygens. In the bridging hydroxyl derivative $[(UO_2)_2(O_2)_4(OH)_2Na_6]$ the two OH^- groups (1- is the *formal* charge) are not bonded to each other (hence the π bond observed in the O_2^{2-}

dimer is absent). In contrast to the peroxide model complex, no covalent interaction was found between U and the OH moieties. Supported by the large negative partial charge of O in OH^-, the U-O(H) bonding was concluded to be of mainly an electrostatic nature.[12]

The cationic $[(UO_2)_2(O_2)(L)_2]^{2+}$ and $[(UO_2)_2(OH)_2(L)_2]^{2+}$ complexes considered in the present work exhibit differences from the neutral $[(UO_2)_2(O_2)_5Na_6]$ and $[(UO_2)_2(O_2)_4(OH)_2Na_6]$ model complexes.[12] The synthesized gas-phase dimer complexes have net charges of 2+ and the TFABDMA ligands are essentially neutral, this in contrast to the four and five O_2^{2-} ions and Na^+ counterions in the two model charge-neutral complexes. A result is that in the complexes prepared here the charge separations are smaller and the bonding conditions are less ionic. In addition, in the 2+ complexes there are no counterions—these are Na^+ ions in the above model complexes—which results in different steric conditions.

The above outlined disparities can lead to differences in the bonding of the $[(UO_2)_2(O_2)(L)_2]^{2+}$ and $[(UO_2)_2(OH)_2(L)_2]^{2+}$ gas-phase complexes as compared to the $[(UO_2)_2(O_2)_5Na_6]$ and $[(UO_2)_2(O_2)_4(OH)_2Na_6]$ model complexes.[12] One visually recognisable difference is the orientation of the OH hydrogens: in the computed structure of $[(UO_2)_2(O_2)_4(OH)_2Na_6]$ the OH hydrogens are in the plane of the U-$(O_{OH})_2$-U moiety[12] (due probably to steric repulsion with the Na^+ ions positioned between the uranyl oxygens). In contrast, in the optimized structure of $[(UO_2)_2(OH)_2(L)_2]^{2+}$ the OH hydrogens are nearly parallel with the uranyl UO bonds. The distance of the OH hydrogens from the uranyl oxygens (2.9 Å) is too large for hydrogen bonding between these atoms, but the parallel arrangement facilitates dipole-dipole interactions, likely stabilizing this orientation of the OH groups.

Selected natural atomic charges and Wiberg bond indices are compiled in Table 3. The natural charges of the ligand O and N atoms (which participate in the donor-acceptor interaction with U) show only negligible differences in the three complexes. This suggests that the outer-sphere ligand-U interactions are essentially independent from the interactions within the di-uranyl core. This conclusion is supported by the close ligand…U distances compiled in Table 2.

Inspection of the atomic charges of the uranyl moieties reveals differences up to 0.07 e and 0.04 e for the charges of U and O, respectively. The U atom is most ionic in $[(UO_2)_2(O)(L)_2]^{2+}$, while least so in $[(UO_2)_2(OH)_2(L)_2]^{2+}$. This correlates well with the net charge of the oxygen and OH bridges between the uranyls, where the negative charge of the single O in $[(UO_2)_2(O)(L)_2]^{2+}$ is the largest, and that of the $(OH)_2$ moiety is the smallest (the large negative atomic charge of O is partly compensated by the positive charge of H in the two bridging OH). These charge differences are, however, quite small and do not introduce considerable differences in the bonding between the uranyl and the bridging moieties. The covalent characters of the complexes, as reflected by the Wiberg bond indices in Table 3, are also very similar. Note that the covalent bond order of 1.0 with the single O in $[(UO_2)_2(O)(L)_2]^{2+}$ is comparable to twice the 0.5 bond order with O_2 and $(OH)_2$ in the other two complexes. Accordingly, none of the other indicated covalent bond orders show notable differences in the three complexes. It is noteworthy that the covalent bond order within the O_2 bridge is 1.0 and that between O and H in the OH moiety is 0.7, while there is no bond

between the two OH moieties. The weak bond in the O_2 bridge is in agreement with the longer O-O distance (1.462 Å; see Table 2) as compared with the neutral O_2 molecule (1.206 Å). This feature can be explained by the occupied anti-bonding orbitals in the negatively charged O_2 bridge.

Selected Kohn-Sham orbitals are shown in Figures 6-8. The main features of Figure 6c and 6d agree with those of the respective orbitals presented for the $[(UO_2)_2(O_2)_5Na_6]$ [12] and $[UO_2]_2(\mu\text{-}\eta^2\text{:}\eta^2\text{-}O_2(H_2O)_6]^{2+}$ [13] models. In $[(UO_2)_2(O_2)(L)_2]^{2+}$ (Figure 6) the main orbital interactions between the UO_2 and O_2 moieties is between the $6d_\delta$, $5f_\delta$ and $5f_\phi$ atomic orbitals of U and antibonding π^* orbitals of O_2. Hence in the dimers the bonding situation is more complex than in the simple $UO_2^+ \ldots O_2$ model, where the bonding was attributed solely to the U 5fϕ - O_2 π^* orbital interaction.[54] This may partly be due to the bent structure requiring hybrid orbital orientations and partly to the effect of ligands polarizing the electron density distribution of U.

The Kohn-Sham orbitals characteristic of bonding in $[(UO_2)_2(OH)_2(L)_2]^{2+}$ (Figure 7) are similar to those of $[(UO_2)_2(O_2)(L)_2]^{2+}$; the main difference is that the π^* of O_2 is replaced by the individual O p orbitals of the OH moieties. These similar covalent and ionic (i.e., close atomic charges, see above) characteristics explain the very similar $U \ldots O_{br}$ distances in $[(UO_2)_2(O_2)(L)_2]^{2+}$ and $[(UO_2)_2(OH)_2(L)_2]^{2+}$.

The $[(UO_2)_2(O)(L)_2]^{2+}$ complex deviates from the other two in that there is only one oxygen bridging the two uranyl moieties. The most striking structural difference is the perpendicular orientation—i.e., a torsional angle of ca. 90^o—of the two UO_2 moieties, as well as of the coordinating TFABDMA ligands. This geometry can be explained on the basis of the molecular orbitals in Figure 8. All three O 2p orbitals participate in orbital interactions with the UO_2 moieties. Most stabilizing is the (lowest-energy) σ bond (Figure 8a) with U 6d orbitals. The other two O 2p orbitals overlap with a π^* anti-bonding orbital of each UO_2 moiety (e.g. Figure 8b) explaining the longest uranyl $U{=}O_{yl}$ bonds found in $[(UO_2)_2(O)(L)_2]^{2+}$ among the three complexes. The orthogonal character of these two latter O 2p orbitals requires a perpendicular relative orientation of the two UO_2 moieties for the optimal interaction. The situation is similar in Figure 8c, where the O 2p atomic orbital interacts with U 5f. For $[(UO_2)_2(O)(L)_2]^{2+}$ the ligand…UO_2 interactions result in a slight 13^o bending of the $U \ldots O_{br} \ldots U$ angle, to ~167^o. The steric strain in this structure is reduced by the perpendicular orientation of the two uranyl moieties.

As mentioned above, the characteristic geometrical parameters of the complexes compiled in Table 2 support the bonding features discussed above. Both the $U{=}O_{yl}$ bond distances and the ligand…U distances differ only marginally in the three complexes. Larger differences can be seen in Table 2 for the parameters within the di-uranyl core due to the three different bridging moieties: O_2/O/$(OH)_2$.

An Evaluation of the Relative Energies of Bent Uranyl Peroxides

The most characteristic, intriguing and relevant structural feature of the studied complexes is the bent $U \ldots O_2 \ldots U$ interaction in $[(UO_2)_2(O_2)(L)_2]^{2+}$. This substantially bent structure, to a dihedral angle of 145^o, is in accord with similarly bent geometries in compounds and nanostructures containing the $(UO_2)_2O_2$ moiety,[18] and is in contrast to the

considerably less bent arrangement in $[(UO_2)_2(OH)_2(L)_2]^{2+}$. In the $[(UO_2)_2(O_2)_4(OH)_2Na_6]$ model complex the U…$(OH)_2$…U moiety is planar (i.e., the dihedral angle is 180°).[12] On the basis of their model calculations, Vlaisavljevich et al. explained the bent feature in the $[(UO_2)_2(O_2)_5Na_6]$ model as due to the presence of Na^+ counterions interacting with the $[(UO_2)_2(O_2)_5]^{6-}$ complex anion: the position of the bridging peroxide was proposed as ensuring the maximum Coulomb interaction between the uranyl oxygens and the Na^+ counterions.[12]

In $[(UO_2)_2(O_2)(L)_2]^{2+}$ and $[(UO_2)_2(OH)_2(L)_2]^{2+}$ there are no counterions between the partially negatively charged uranyl oxygens. Hence, instead of a Coulomb attraction, a repulsion is expected. Yet, $[(UO_2)_2(O_2)(L)_2]^{2+}$ has the same (145°) U…O_2…U dihedral angle as was computed for $[(UO_2)_2(O_2)_5Na_6]$. The U…$(OH)_2$…U dihedral angle in $[(UO_2)_2(OH)_2(L)_2]^{2+}$ is somewhat larger (162°), with the structure substantially closer to planar. The two close-lying uranyl oxygens—those facing down in the Fig. 5 top and bottom structures—are at a distance of 3.3 Å from each other in both $[(UO_2)_2(O)(L)_2]^{2+}$ and $[(UO_2)_2(OH)_2(L)_2]^{2+}$. This distance is somewhat larger than the sum of the van der Waals radii of the two oxygen atoms (3.04 Å).[56,57]

The O_2 bridge in $[(UO_2)_2(O_2)(L)_2]^{2+}$ cannot induce dihedral bending because the main orbital interactions are established by the planar π* orbital (see Figure 6). In addition, the Coulomb interactions would prefer a symmetric D_{2h} arrangement for the $(UO_2)_2(O_2)$ moiety. This hypothesis was evaluated by computations on the elementary model $[(UO_2)_2(O_2)]^{2+}$ complex that does not have the terminal TFABDMA ligands that are necessary to stabilize the dipositive charge complex from solution to gas in the experiments. The optimization converged to a D_{2h} structure with a U…(O_2)…U dihedral angle of 180° and uranyl O…O distances of 4.57 Å; the structure is shown in Figure 9. The peroxide moiety is essential for bridging the otherwise strongly repulsive (2+ charged) U atoms. The UO_2 moieties are slightly bent away from each other with the two O_{yl}=U=O_{yl} angles being 172°. The torsional angle defines the staggering between the negatively-charged O_{yl} atoms on the two uranyls, as defined in SI Figure S2: eclipsed O-atoms on the two uranyls corresponds to a torsional angle of 0°.

It is concluded that the dihedral angle in $[(UO_2)_2(O_2)]^{2+}$ is 180° (i.e., planar) whereas that in $[(UO_2)_2(O_2)(L)_2]^{2+}$ is 145° (i.e., bent by 35°); this latter value is comparable to the degree of bending (140°) in studtite and also in several uranyl cage structures.[1,58] To evaluate the inherent flexibility of the elementary uranyl peroxide moiety, the energetics of the very simple model complex, $[(UO_2)_2(O_2)]^{2+}$, were assessed as a function of the dihedral angle. The structure of $[(UO_2)_2(O_2)]^{2+}$ was constrained as C_{2v} and the relative energy was computed as the U…O_2…U dihedral angle deviates from the value of 180° found in the lowest-energy structure. The results, shown in Figure 9 (and Fig. S1), reveal that the energy does not increase significantly (< 1 kJ/mol) for deviations from planarity of up to 20° (dihedral angles down to 160°) and the energy increase remains minor (<10 kJ/mol) for bending of up to 40° (dihedral angles down to 140°, which is that found in studtite). The energy increase is only ~5 kJ/mol for a dihedral angle of 145°, which is that computed for the $[(UO_2)_2(O_2)(L)_2]^{2+}$ complex. It is apparent that the structure of the uranyl peroxide moiety is inherently planar but that substantial deviations from planarity, which enables the formation of cage structures,

can occur due to only minor energy perturbations, such as may be introduced by counterions, neutral ligands or crystal packing. This was also evident in the small $[UO_2]_2(\mu\text{-}\eta^2\text{:}\eta^2\text{-}O_2(H_2O)_6]^{2+}$ model evaluated by Miró et al.,[13] where the H_2O ligands stabilized the bent structure by 2 kJ/mol.

The imposition of C_{2v} symmetry in our computations for $[(UO_2)_2(O_2)]^{2+}$ mandates that the torsional angle between the uranyl moieties be 0^o (i.e., an eclipsed geometry with the minimum $O_{yl}\ldots O_{yl}$ distance). To assess the propensity for deviations of the torsional angle from 0^o as a means to reduce $O_{yl}\ldots O_{yl}$ repulsion, this angle was initially set at 10^o for a large dihedral angle of 120^o. This structure relaxed to the lowest energy structure with a torsional angle of 0^o. Somewhat surprisingly, the torsional angle does not deviate from 0^o, at least not for $U\ldots O_2\ldots U$ torsional angles down to highly bent 120^o. The minimum character this structure is supported by the lack of any computed imaginary frequency.

We conclude that the bent structure of $[(UO_2)_2(O_2)(L)_2]^{2+}$ originates from interactions with the TFABDMA ligands. From the two donor-acceptor interactions, that with C=O is expected to favor a planar arrangement due to the orientation of the O lone pairs. The lone pair of N, however, is not in this plane and its orientation depends on the torsion of the ligand. Another ligand$\ldots UO_2$ interaction in $[(UO_2)_2(O_2)(L)_2]^{2+}$ and $[(UO_2)_2(OH)_2(L)_2]^{2+}$ is weak hydrogen bonding between the uranyl downward oxygens and the close lying (2.6 Å) two NCH_2 hydrogens; there are also repulsive interactions between the upper uranyl oxygens and the CF_3 group. The latter interaction is absent in higher-energy conformers with CF_3 turned away, but the bent character (though with somewhat larger dihedral angle) is preserved.

The computed relative energies for $[(UO_2)_2(O_2)]^{2+}$ as a function of dihedral angle (Fig. 9) indicate that an interaction of only ~5 kJ/mol between the TFABDMA ligands in $[(UO_2)_2(O_2)(L)_2]^{2+}$ could induce the substantial bending to a dihedral angle of 145^o. The conclusions from the present work are in accord with those from Qui et al.[18], who studied several uranyl peroxide dimers and concluded that only minimal energy perturbations—on the order of 10 kJ/mol—induced by counterions and other effects are needed to induce the observed bending of the dihedral angle. The present results demonstrate the inherently planar nature of the simplest $[(UO_2)_2(O_2)]^{2+}$ dimer, and the substantial deviation from planarity introduced by the addition of terminal neutral ligands.

Summary

A gas-phase uranyl peroxide dimer, $[(UO_2)_2(O_2)(L)_2]^{2+}$, was synthesized by ESI. The mechanism for the formation of this novel gas-phase dimer is uncertain. It is notable that this species forms without addition of peroxide to the ESI solution. This suggests a sufficiently high stability that the dimer is formed by reaction with molecular O_2. The high stability of the peroxide dimer is further indicated by its unreactive character towards O_2 or H_2O in the gas phase. CID of the dimer results in endothermic O-atom elimination to produce $[(UO_2)_2(O)(L)_2]^{2+}$, which undergoes spontaneous exothermic chemisorption of H_2O to yield the hydroxide dimer, $[(UO_2)_2(OH)_2(L)_2]^{2+}$. The energetics for the experimentally observed processes are in accord with DFT computations. The computed structure of $[(UO_2)_2(O_2)(L)_2]^{2+}$ features a bent uranyl-peroxide-uranyl moiety, with a dihedral angle of

145^{o} between the planes defined by the two U-O_2 linkages. To evaluate the intrinsic structure and energetics required for bending of uranyl peroxides, computations were also performed for $[(UO_2)_2(O_2)]^{2+}$, which is the most elementary of the model gas-phase uranyl peroxide complexes. The results reveal that the inherently most stable geometry is planar, with a dihedral angle of 180^{o}, and that substantial deviations from planarity, up to 40^{o}, are induced by energy perturbations of 10 kJ/mol or less. This finding is in accord with previous conclusions that stable uranyl peroxide cage structures are not formed due to an inherently bent nature of the uranyl-peroxide-uranyl moiety, but rather result from the minor energy needed to distort this moiety from intrinsic planarity, such as by interactions with counterions. The results reported here represent the first synthesis and reactivity studies of a gas-phase uranyl peroxide dimer. The agreement between observed gas-phase reactivity and DFT predictions provide validation of the latter, and confidence in other computed properties.

Supporting Information

Elaborated version of Figure 9; definition of the torsional angle in uranyl dimers; Cartesian coordinates of computed structures for the three dimer structures shown in Figure 5.

Acknowledgements

This work was supported by the U.S. Department of Energy, Office of Basic Energy Sciences, Heavy Element Chemistry, at LBNL under Contract No. DE-AC02-05CH11231 [P.D.D., P.V.D., L.R. and J.K.G].

Table 1. Calculated reaction energies (kJ/mol).

	ΔH^0	ΔH^{298}	ΔG^{298}
Reaction (3) / Elimination of O from $[(UO_2)_2(O_2)(L)_2]^{2+}$	228.9	232.8	189.2
Reaction (4) / Addition of H_2O to $[(UO_2)_2(O)(L)_2]^{2+}$	-133.1	-137.5	-86.5

Table 2. Selected calculated geometrical parameters.

Parameter[a]	$[(UO_2)_2(O_2)(L)_2]^{2+}$	$[(UO_2)_2(O)(L)_2]^{2+}$	$[(UO_2)_2(OH)_2(L)_2]^{2+}$	$[(UO_2)_2O_2]^{2+}$
$U=O_{yl}$	1.774,[b] 1.757	1.767,[b] 1.782	1.762, 1.777[b] 1.757, 1.771[b]	1.723
O_{br}-O_{br}	1.462	-	2.749	1.460
$O_{yl}\ldots O_{yl}$	5.464,[b] 3.322	4.75	4.389,[b] 3.291	4.572
$U\ldots O_{br}$	2.330, 2.333	2.108	2.357, 2.362 2.352, 2.356	2.299
$U\ldots O_{br}\ldots U$	129.9, 130.0	166.7	106.7	172.6
$U\ldots O_{br}$-$O_{br}\ldots U$	145.4	-	162.1	180.0
O_{yl}=U-U=O_{yl}	0.0°	91.4°	0.8°	0.0°
$U\ldots O=C_{lig}$	2.378, 2.402	2.376, 2.400	2.391, 2.415 2.397, 2.418	-
$U\ldots N_{lig}$	2.807	2.798	2.863, 2.872	-
O_{br}-H	-	-	0.964	-
$O_{yl}\ldots$H-O_{br}	-	-	2.9	-

[a]The indexes 'br' and 'lig' indicate bridging and coordinating groups of the TFABDMA ligand, respectively. O_{yl} denotes a uranyl oxygen atom. In $[(UO_2)_2(O_2)(L)_2]^{2+}$ there is a slight asymmetry because of the CF_3 orientation. In some cases average distances can be used because the difference is very small; for $[(UO_2)_2(O_2)(L)_2]^{2+}$ the optimisations stopped at a slightly asymmetric structure because of the low forces and no application of symmetry constraints.

[b]Distances involving O_{yl} atoms with up orientation in Figure 5.

Table 3. Selected results from the NBO analysis.

Parameter[a]	$[(UO_2)_2(O_2)(L)_2]^{2+}$	$[(UO_2)_2(O)(L)_2]^{2+}$	$[(UO_2)_2(OH)_2(L)_2]^{2+}$
n(U)	1.99	2.03	1.96
$n(O_{yl})$	-0.62,[b] -0.55	-0.62, -0.56	-0.59,[b] -0.61
$n(O_{br})$	-0.41	-0.85	-0.92
$n(O_{br})_2$, $n(O_{br}H)_2$	-0.82	-	-0.76
$n(H_{br})$	-	-	+0.54
$n(O_{lig})$	-0.66	-0.66	-0.65
$n(N_{lig})$	-0.54	-0.54	-0.53
$W(U{=}O_{yl})$	2.0,[b] 2.1	2.0,[b] 2.1	2.1,[b] 2.0
$W(U\ldots O_{br})$	0.5	1.0	0.5
$W(O_{br}\text{-}O_{br})$	1.0	-	-
$W(O_{br}\text{-}H)$	-	-	0.7
$W(U\ldots O_{lig})$	0.4	0.4	0.4
$W(U\ldots N_{lig})$	0.2	0.2	0.2

[a]The indexes 'uranyl', 'br' and 'lig' indicate uranyl, bridging and coordinating groups of the TFABDMA ligand, respectively. O_{yl} indicates a uranyl O atom. n is the natural atomic charge. W is the Wiberg bond index.
[b]Distances involving O_{yl} atoms with up orientation in Figure 5.

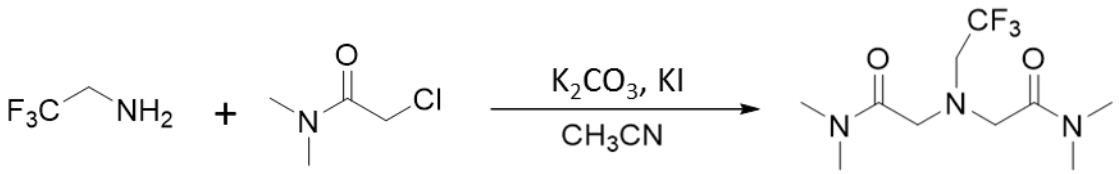

Scheme 1. Synthesis of the TFABDMA ligand (H atoms are not shown).

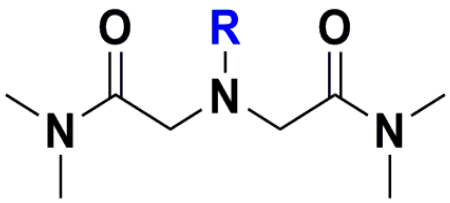

Figure 1. The generic structure of diamide amine-functionalized ligands. For the TFABDMA ligand (L) employed in the present work, **R** = CH_2CF_3 and the net formula is $C_{10}H_{18}N_3O_2F_3$ with a mass of 269 Da.

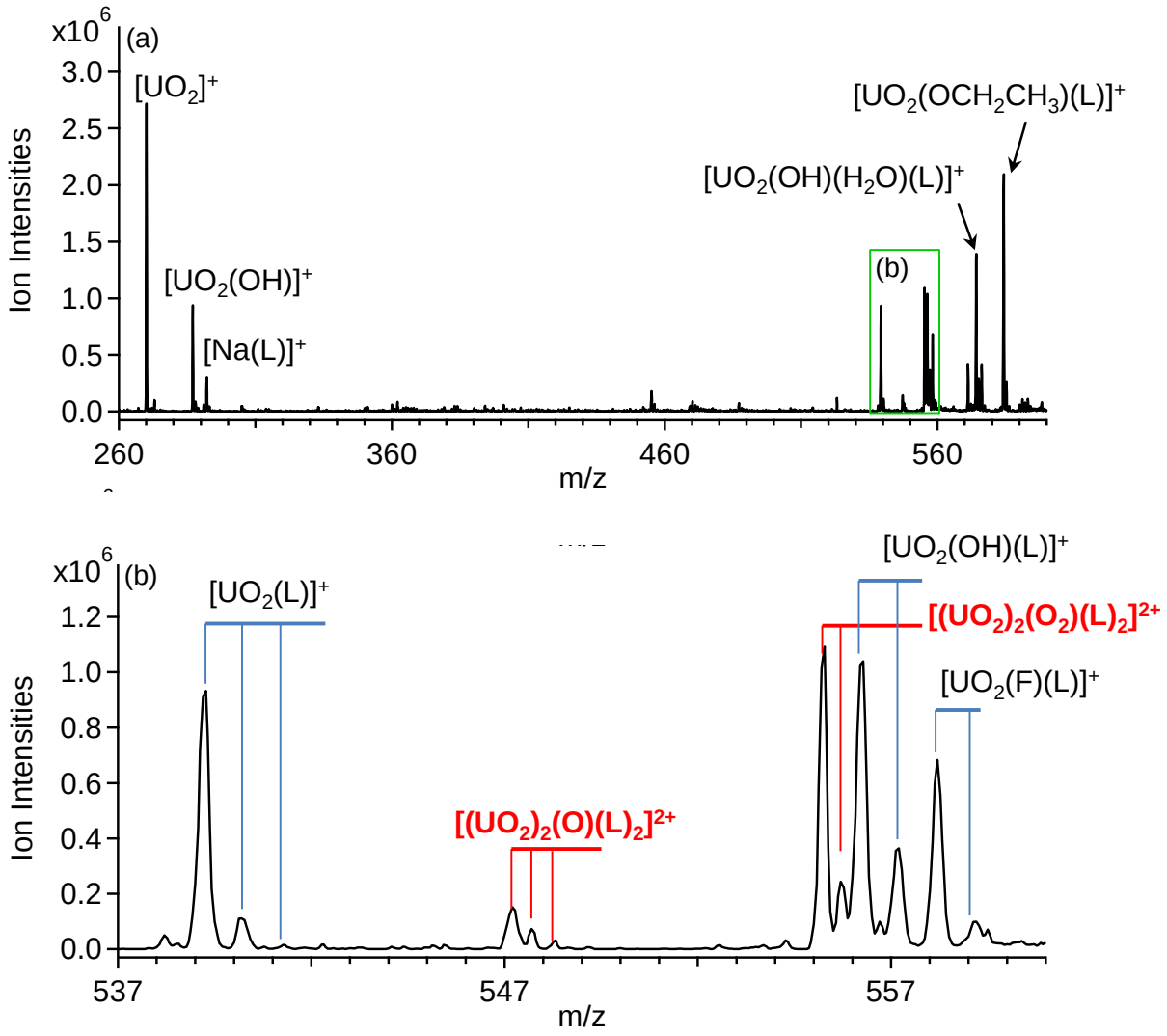

Figure 2. (a) ESI mass spectrum for the uranyl/L solution (L = TFABDMA). (b) Expansion of the peaks in the green box in (a). The assignments of charge state z are based on m/z separations of 1 for z = 1+ ions and 0.5 for z = 2+ ions. The assignments are confirmed by the CID mass spectra (Fig. 3).

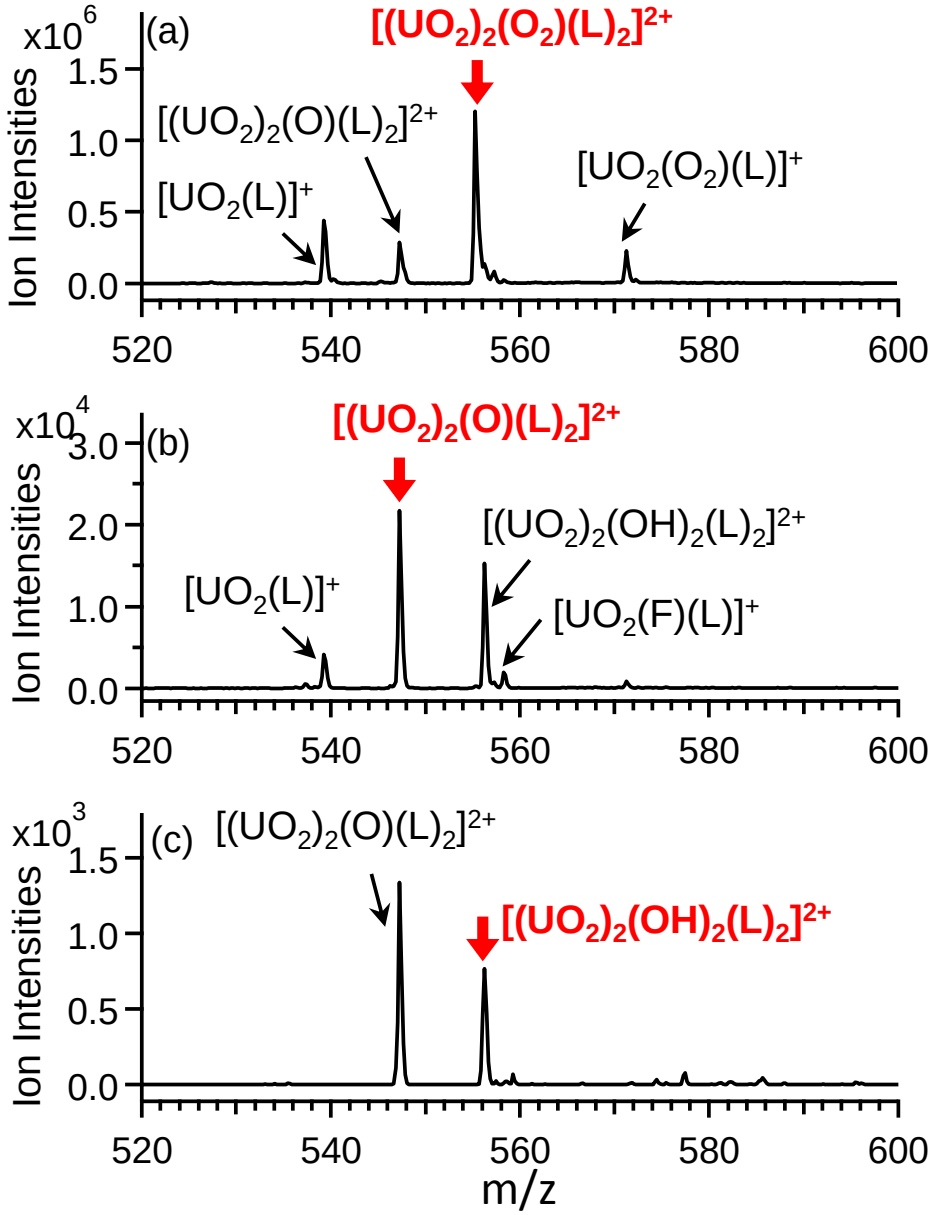

Figure 3. CID mass spectra of complexes identified in red. The nominal CID voltages of (a) 0.6, (b) 0.5 and (c) 0.25 were selected to identify the dominant pathways, not to evaluate the fragmentation energies.

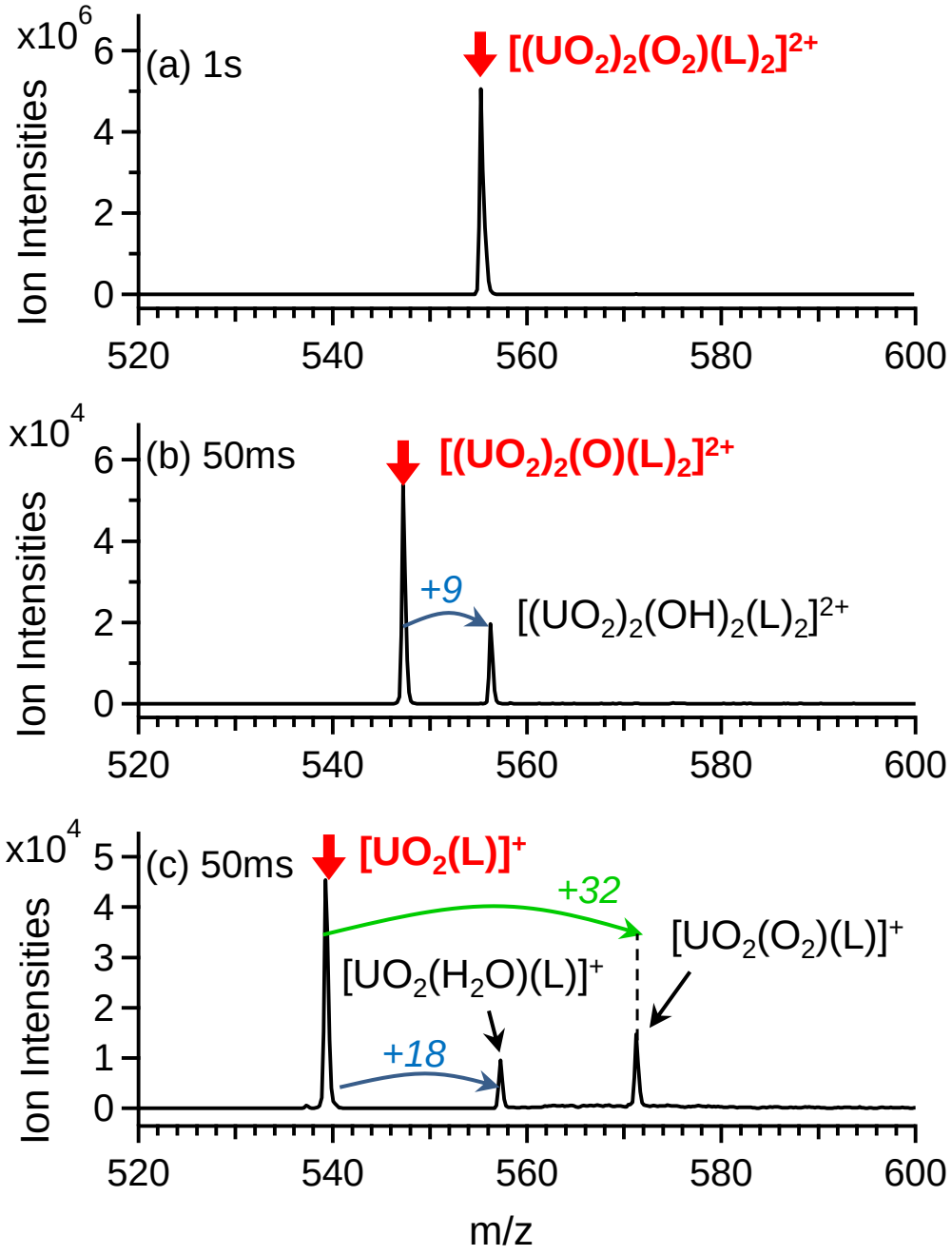

Figure 4. Mass spectra acquired after isolation of the complexes indicated in red for (a) 1000 ms, (b) 50 ms and (c) 50 ms. The observed reactions are with background H_2O and O_2 in the ion trap; the background reactant pressures are constant to within 10%.

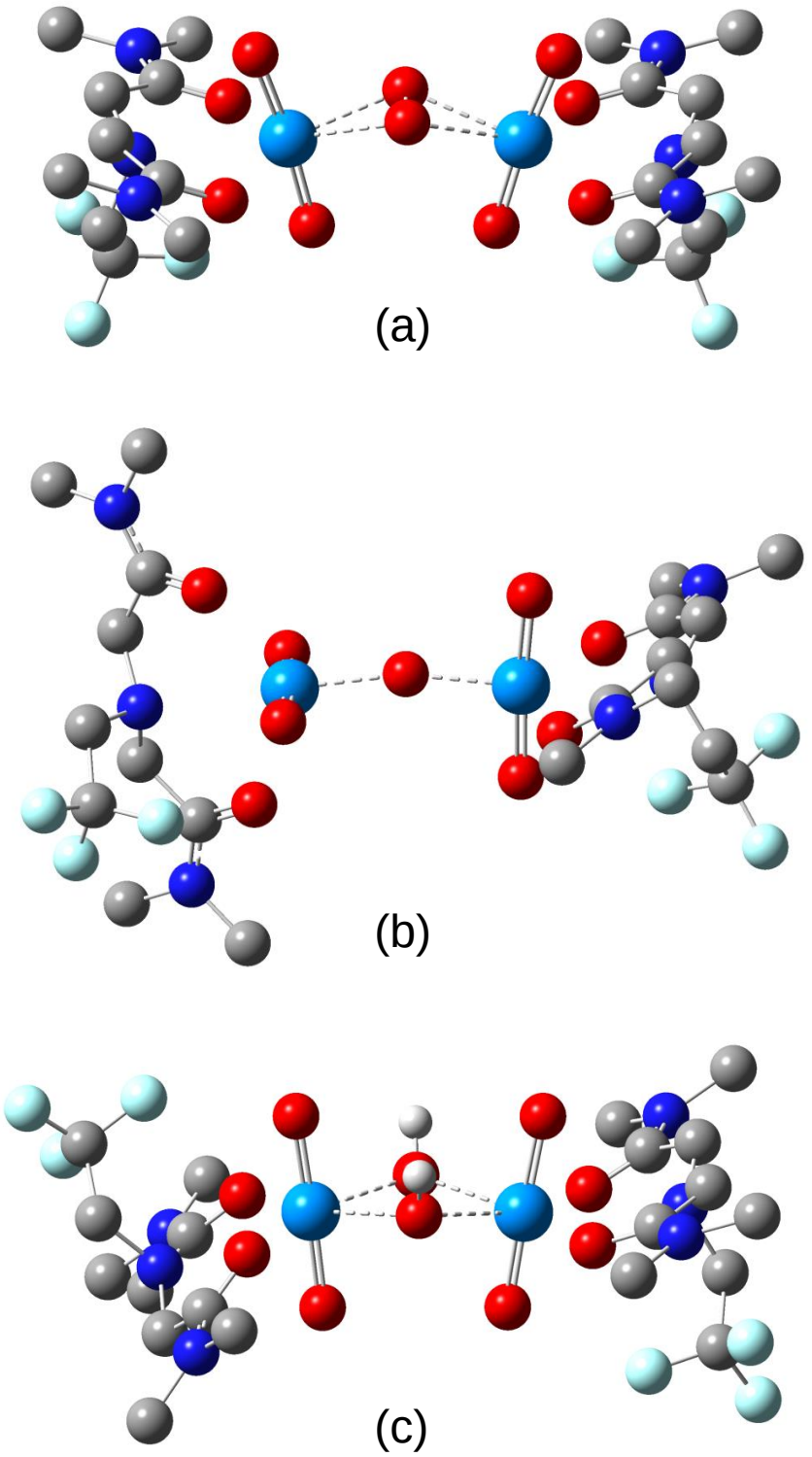

Figure 5. Computed lowest energy dimer structures: (a) $[(UO_2)_2(O_2)(L)_2]^{2+}$; (b) $[(UO_2)_2(O)(L)_2]^{2+}$; (c) $[(UO_2)_2(OH)_2(L)_2]^{2+}$. Red = O; dark blue = N; light blue = U; lightest blue = F; grey = C; shaded = H. The H atoms on the organic ligands are not shown. The dihedral angle in (a) and (c) is that between the planes defined by the U…O_2 coordination.

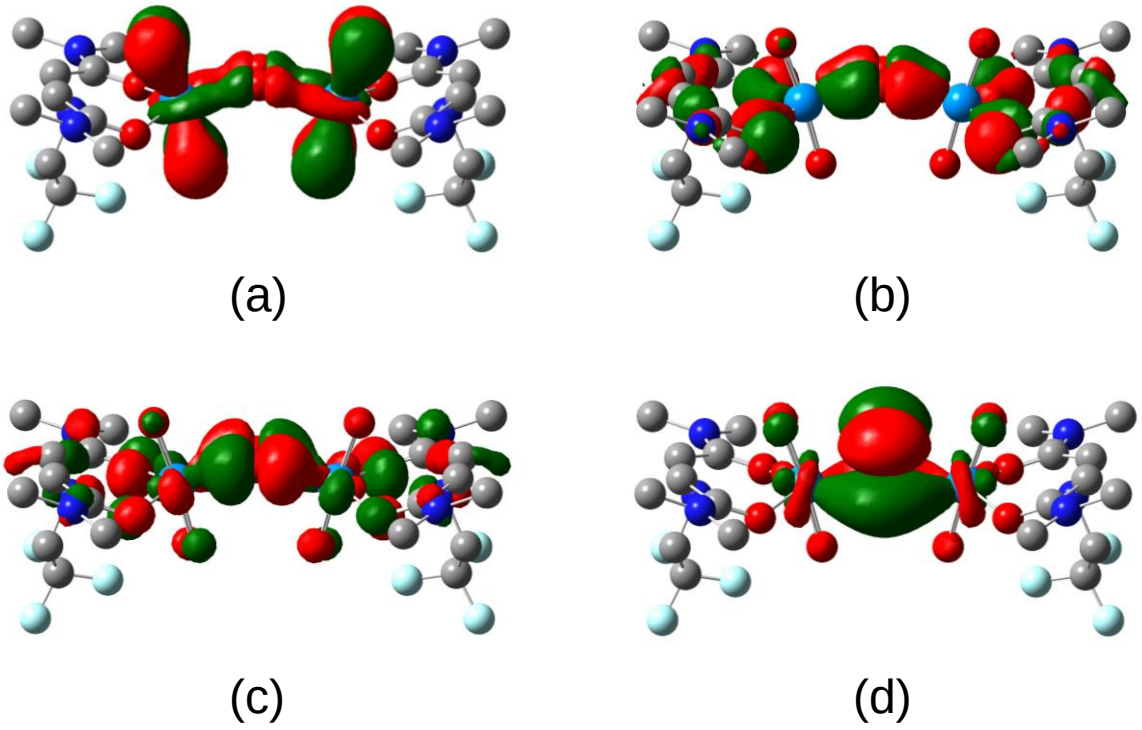

Figure 6. Selected Kohn-Sham orbitals for $[(UO_2)_2(O_2)(L)_2]^{2+}$: (a) πUO_2 + U…π^*O_2; (b) U…π^*O_2 + πC=O…U; (c) minor U…π^*O_2; (d) π^*O_2…U.

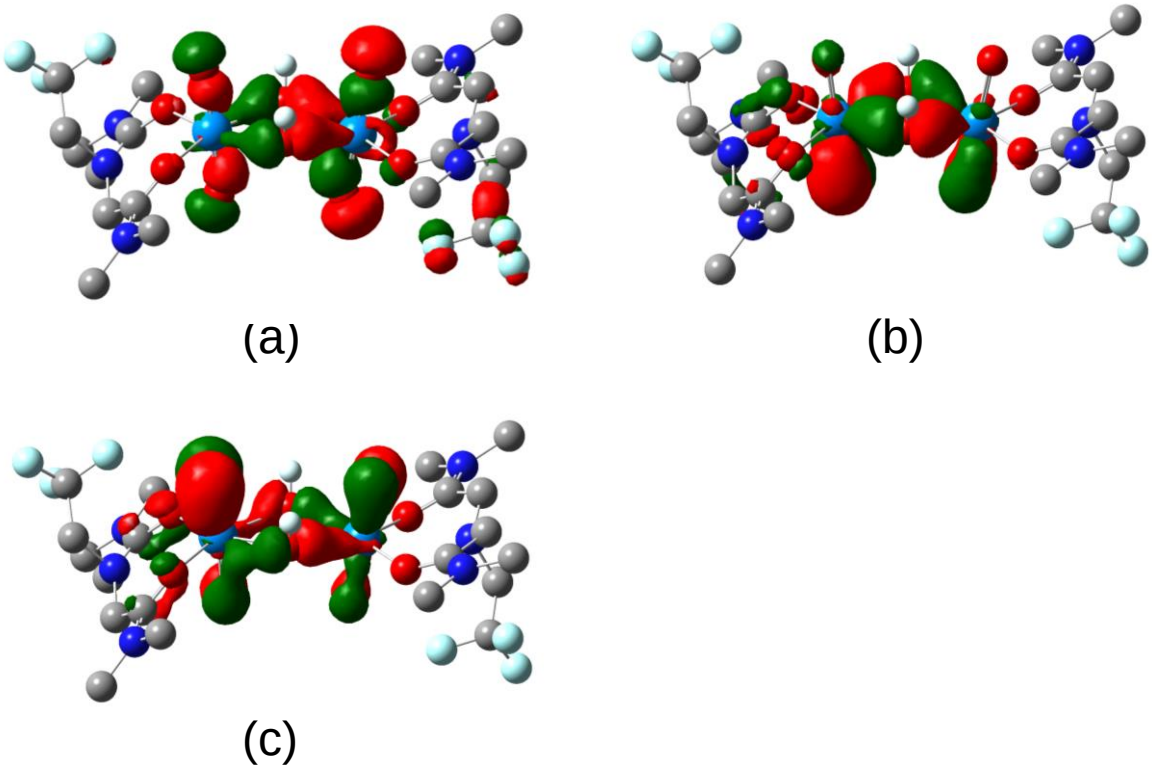

Figure 7. Selected Kohn-Sham orbitals for $[(UO_2)_2(OH)_2(L)_2]^{2+}$: (a) $\sigma U\ldots O_{br} + \sigma UO_2$; (b) $\sigma U\ldots O_{br} + \pi UO_2$; (c) $\pi UO_2 + \sigma U\ldots O_{br}$.

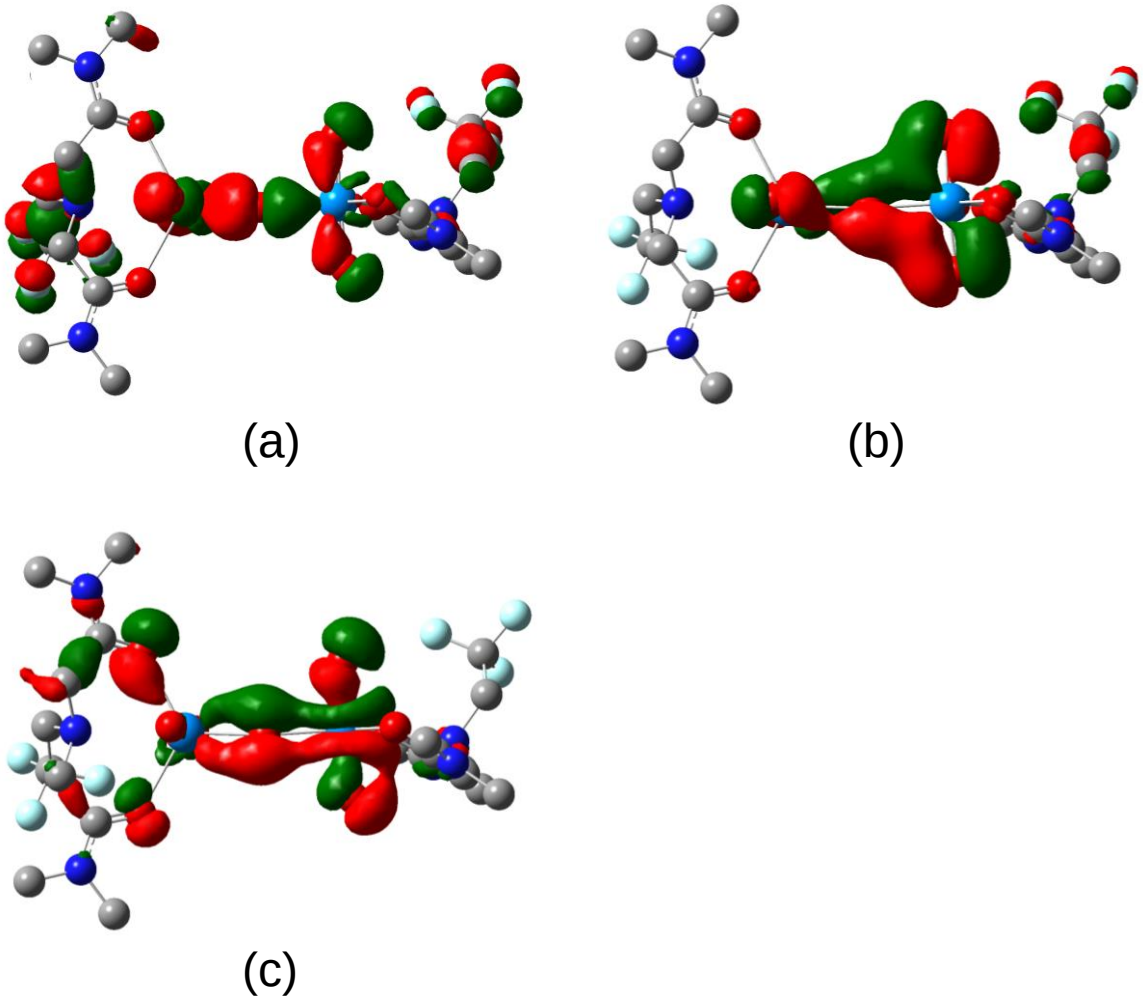

Figure 8. Selected Kohn-Sham orbitals for $[(UO_2)_2(O)(L)_2]^{2+}$: (a) $\sigma U\ldots O_{br}$; (b) πUO_2 + $\pi U\ldots O_{br}$; (c) $\pi U\ldots O_{br}$.

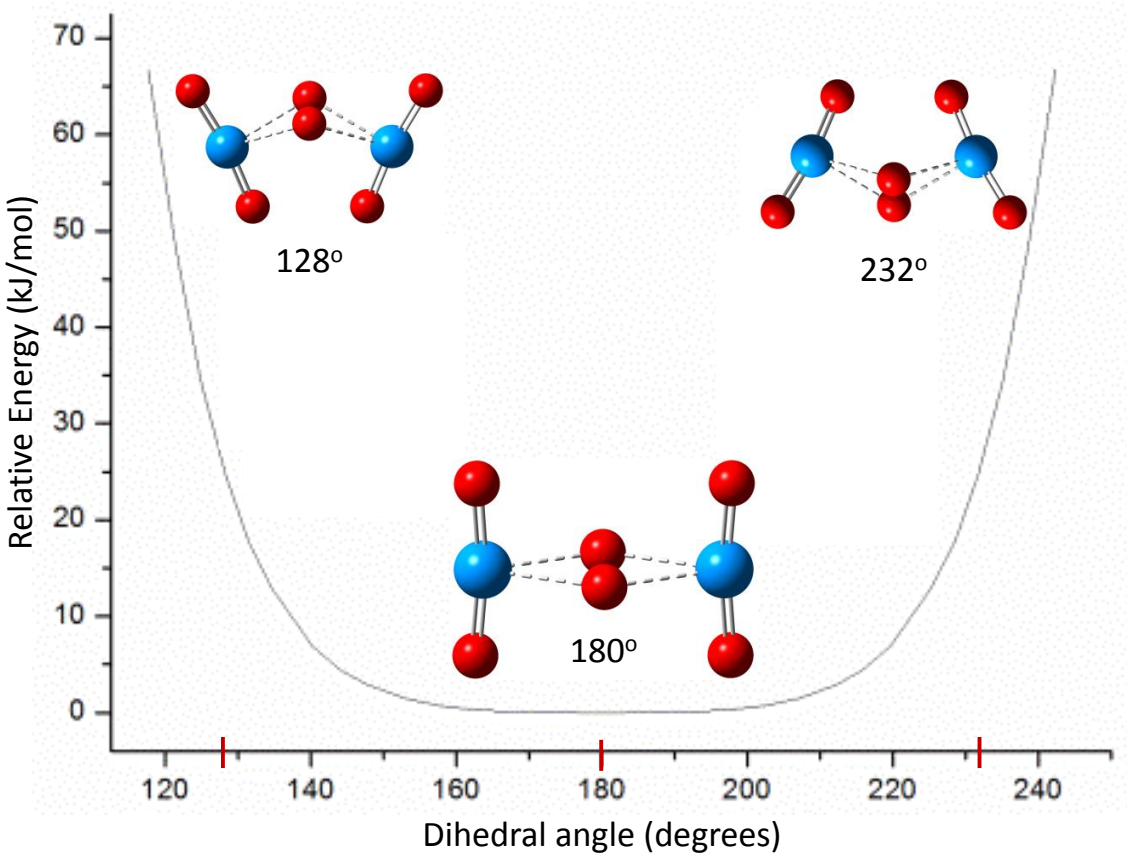

Figure 9. Computed energies of the $[(UO_2)_2(O_2)]^{2+}$ complex, which is the observed $[(UO_2)_2(O_2)(L)_2]^{2+}$ ligated complex shown in Figure 5, but without the terminal organic ligands L. The energy is shown as a function of the dihedral angle, where 180° corresponds to a planar U…O_2…U structure shown in the middle. The structures corresponding to bent dihedral angles of 128° and 232° are also shown; these two geometries (and their relative energies) are the same except for inversion of the dihedral angle. The computed dihedral angle of the ligated complex studied in the experiments is 145°.

References

(1) Burns, P. C.; Hughes, K. A.: Studtite, [(UO2)(O-2)(H2O)(2)](H2O)(2): The first structure of a peroxide mineral. *American Mineralogist* **2003**, *88*, 1165-1168.

(2) Burns, P. C.; Kubatko, K. A.; Sigmon, G.; Fryer, B. J.; Gagnon, J. E.; Antonio, M. R.; Soderholm, L.: Actinyl peroxide nanospheres. *Angewandte Chemie-International Edition* **2005**, *44*, 2135-2139.

(3) Sigmon, G. E.; Ling, J.; Unruh, D. K.; Moore-Shay, L.; Ward, M.; Weaver, B.; Burns, P. C.: Uranyl-Peroxide Interactions Favor Nanocluster Self-Assembly. *Journal of the American Chemical Society* **2009**, *131*, 16648-16649.

(4) Ling, J.; Qiu, J.; Sigmon, G. E.; Ward, M.; Szymanowski, J. E. S.; Burns, P. C.: Uranium Pyrophosphate/Methylenediphosphonate Polyoxometalate Cage Clusters. *Journal of the American Chemical Society* **2010**, *132*, 13395-13402.

(5) Unruh, D. K.; Ling, J.; Qiu, J.; Pressprich, L.; Baranay, M.; Ward, M.; Burns, P. C.: Complex Nanoscale Cage Clusters Built from Uranyl Polyhedra and Phosphate Tetrahedra. *Inorganic Chemistry* **2011**, *50*, 5509-5516.

(6) Qiu, J.; Ling, J.; Sui, A.; Szymanowski, J. E. S.; Simonetti, A.; Burns, P. C.: Time-Resolved Self-Assembly of a Fullerene-Topology Core-Shell Cluster Containing 68 Uranyl Polyhedra. *Journal of the American Chemical Society* **2012**, *134*, 1810-1816.

(7) Qiu, J.; Burns, P. C.: Clusters of Actinides with Oxide, Peroxide, or Hydroxide Bridges. *Chemical Reviews* **2013**, *113*, 1097-1120.

(8) Qiu, J.; Ling, J.; Sieradzki, C.; Nguyen, K.; Wylie, E. M.; Szymanowski, J. E. S.; Burns, P. C.: Expanding the Crystal Chemistry of Uranyl Peroxides: Four Hybrid Uranyl-Peroxide Structures Containing EDTA. *Inorganic Chemistry* **2014**, *53*, 12084-12091.

(9) Kroto, H. W.; Heath, J. R.; Obrien, S. C.; Curl, R. F.; Smalley, R. E.: C-60 - Buckminsterfullerene. *Nature* **1985**, *318*, 162-163.

(10) Wylie, E. M.; Peruski, K. M.; Prizio, S. E.; Bridges, A. N. A.; Rudisill, T. S.; Hobbs, D. T.; Phillip, W. A.; Burns, P. C.: Processing used nuclear fuel with nanoscale control of uranium and ultrafiltration. *Journal of Nuclear Materials* **2016**, *473*, 125-130.

(11) Armstrong, C. R.; Nyman, M.; Shvareva, T.; Sigmon, G. E.; Burns, P. C.; Navrotsky, A.: Uranyl peroxide enhanced nuclear fuel corrosion in seawater. *Proceedings of the National Academy of Sciences of the United States of America* **2012**, *109*, 1874-1877.

(12) Vlaisavljevich, B.; Gagliardi, L.; Burns, P. C.: Understanding the Structure and Formation of Uranyl Peroxide Nanoclusters by Quantum Chemical Calculations. *J. Am. Chem. Soc.* **2010**, *132*, 14503-14508.

(13) Miró, P.; Pierrefixe, S.; Gicquel, M.; Gil, A.; Bo, C.: On the Origin of the Cation Templated Self-Assembly of Uranyl-Peroxide Nanoclusters. *Journal of the American Chemical Society* **2010**, *132*, 17787-17794.

(14) Miró, P.; Bo, C.: Uranyl-Peroxide Nanocapsules: Electronic Structure and Cation Complexation in [(UO2)(20)(mu-O-2)(30)](20-). *Inorganic Chemistry* **2012**, *51*, 3840-3845.

(15) Gil, A.; Karhanek, D.; Miró, P.; Antonio, M. R.; Nyman, M.; Bo, C.: A Journey inside the U28 Nanocapsule. *Chemistry-a European Journal* **2012**, *18*, 8340-8346.

(16) Buhl, M.; Sieffert, N.; Wipff, G.: Structure of a uranyl peroxo complex in aqueous solution from first-principles molecular dynamics simulations. *Dalton Transactions* **2014**, *43*, 11129-11137.

(17) Miró, P.; Vlaisavljevich, B.; Dzubak, A. L.; Hu, S. X.; Burns, P. C.; Cramer, C. J.; Spezia, R.; Gagliardi, L.: Uranyl-Peroxide Nanocapsules in Aqueous Solution: Force Field Development and First Applications. *Journal of Physical Chemistry C* **2014**, *118*, 24730-24740.

(18) Qiu, J.; Vlaisavljevich, B.; Jouffret, L.; Nguyen, K.; Szymanowski, J. E. S.; Gagliardi, L.; Burns, P. C.: Cation Templating and Electronic Structure Effects in Uranyl Cage Clusters Probed by the Isolation of Peroxide-Bridged Uranyl Dimers. *Inorg. Chem.* **2015**, *54*, 4445-4455.

(19) Zanonato, P. L.; Di Bernardo, P.; Vallet, V.; Szabo, Z.; Grenthe, I.: Alkali-metal ion coordination in uranyl(VI) poly-peroxide complexes in solution. Part 1: the Li+, Na+ and K+ - peroxide-hydroxide systems. *Dalton Transactions* **2015**, *44*, 1549-1556.

(20) Miró, P.; Vlaisavljevich, B.; Gil, A.; Burns, P. C.; Nyman, M.; Bo, C.: Self-Assembly of Uranyl-Peroxide Nanocapsules in Basic Peroxidic Environments. *Chemistry-a European Journal* **2016**, *22*, 8571-8578.

(21) Masci, B.; Thuery, P.: Uranyl complexes with the pyridine-2,6-dicarboxylato ligand: new dinuclear species with mu-eta(2), eta(2)-peroxide, mu(2)-hydroxide or mu(2)-methoxide bridges. *Polyhedron* **2005**, *24*, 229-237.

(22) Kubatko, K. A.; Forbes, T. Z.; Klingensmith, A. L.; Burns, P. C.: Expanding the crystal chemistry of uranyl peroxides: Synthesis and structures of Di- and triperoxodioxouranium(VI) complexes. *Inorganic Chemistry* **2007**, *46*, 3657-3662.

(23) Alcock, N. W.: Crystal and Molecular Structure of Sodium Uranyl Triperoxide. *Journal of the Chemical Society A -Inorganic Physical Theoretical* **1968**, 1588-1594.

(24) Unruh, D. K.; Burtner, A.; Burns, P. C.: Expanding the Crystal Chemistry of Actinyl Peroxides: mu-eta(2):eta(1) Peroxide Coordination in Trimers of U6+ Polyhedra. *Inorganic Chemistry* **2009**, *48*, 2346-2348.

(25) Goff, G. S.; Brodnax, L. F.; Cisneros, M. R.; Peper, S. M.; Field, S. E.; Scoft, B. L.; Runde, W. H.: First identification and thermodynamic characterization of the ternary U(VI) species, UO2(O-2)(CO3)(2)(4-), in UO2-H2O2-K2CO3 solutions. *Inorganic Chemistry* **2008**, *47*, 1984-1990.

(26) O'Hair, R. A. J.: The 3D quadrupole ion trap mass spectrometer as a complete chemical laboratory for fundamental gas-phase studies of metal mediated chemistry. *Chemical Communications* **2006**, 1469-1481.

(27) Bohme, D. K.; Schwarz, H.: Gas-phase catalysis by atomic and cluster metal ions: The ultimate single-site catalysts. *Angewandte Chemie-International Edition* **2005**, *44*, 2336-2354.

(28) Dau, P. V.; Zhang, Z. C.; Dau, P. D.; Gibson, J. K.; Rao, L. F.: Thermodynamic study of the complexation between Nd3+ and functionalized diacetamide ligands in solution. *Dalton Transactions* **2016**, *45*, 11968-11975.

(29) Gong, Y.; Hu, H. S.; Tian, G. X.; Rao, L. F.; Li, J.; Gibson, J. K.: A Tetrapositive Metal Ion in the Gas Phase: Thorium(IV) Coordinated by Neutral Tridentate Ligands. *Angewandte Chemie-International Edition* **2013**, *52*, 6885-6888.

(30) Gibson, J. K.; Hu, H. S.; Van Stipdonk, M. J.; Berden, G.; Oomens, J.; Li, J.: Infrared Multiphoton Dissociation Spectroscopy of a Gas-Phase Complex of Uranyl and 3-Oxa-Glutaramide: An Extreme Red-Shift of the [O=U=O](2+) Asymmetric Stretch. *Journal of Physical Chemistry A* **2015**, *119*, 3366-3374.

(31) Dau, P. V.; Kim, M.; Garibay, S. J.; Muench, F. H. L.; Moore, C. E.; Cohen, S. M.: Single-Atom Ligand Changes Affect Breathing in an Extended Metal-Organic Framework. *Inorg. Chem.* **2012**, *51*, 5671-5676.

(32) Gong, Y.; Gibson, J. K.: Formation and Characterization of the Uranyl-SO2 Complex, UO2(CH3SO2)(SO2)(-). *Journal of Physical Chemistry A* **2013**, *117*, 783-787.

(33) Rios, D.; Rutkowski, P. X.; Shuh, D. K.; Bray, T. H.; Gibson, J. K.; Van Stipdonk, M. J.: Electron transfer dissociation of dipositive uranyl and plutonyl coordination complexes. *Journal of Mass Spectrometry* **2011**, *46*, 1247-1254.

(34) Gronert, S.: Estimation of effective ion temperatures in a quadrupole ion trap. *Journal of the American Society for Mass Spectrometry* **1998**, *9*, 845-848.

(35) Rios, D.; Michelini, M. C.; Lucena, A. F.; Marçalo, J.; Bray, T. H.; Gibson, J. K.: Gas-Phase Uranyl, Neptunyl, and Plutonyl: Hydration and Oxidation Studied by Experiment and Theory. *Inorganic Chemistry* **2012**, *51*, 6603-6614.

(36) Frisch, M. J.; Trucks, G. W.; Schlegel, H. B.; Scuseria, G. E.; Robb, M. A.; Cheeseman, J. R.; Scalmani, G.; Barone, V.; Mennucci, B.; Petersson, G. A.; Nakatsuji, H.; Caricato, M.; Li, X.; Hratchian, H. P.; Izmaylov, A. F.; Bloino, J.; Zheng, G.; Sonnenberg, J. L.; Hada, M.; Ehara, M.; Toyota, K.; Fukuda, R.; Hasegawa, J.; Ishida, M.; Nakajima, T.; Honda, Y.; Kitao, O.; Nakai, H.; Vreven, T.; Montgomery Jr., J. A.; Peralta, J. E.; Ogliaro, F.; Bearpark, M.; Heyd, J. J.; Brothers, E.; Kudin, K. N.; Staroverov, V. N.; Keith, T.; Kobayashi, R.; Normand, J.; Raghavachari, K.; Rendell, A.; Burant, J. C.; Iyengar, S. S.; Tomasi, J.; Cossi, M.; Rega, N.; Millam, J. M.; Klene, M.; Knox, J. E.; Cross, J. B.; Bakken, V.; Adamo, C.; Jaramillo, J.; Gomperts, R.; Stratmann, R. E.; Yazyev, O.; Austin, A. J.; Cammi, R.; Pomelli, C.; Ochterski, J. W.; Martin, R. L.; Morokuma, K.; Zakrzewski, V. G.; Voth, G. A.; Salvador, P.; Dannenberg, J. J.; Dapprich, S.; Daniels, A. D.; Farkas, O.; Foresman, J. B.; Ortiz, J. V.; Cioslowski, J.; Fox, D. J.: Gaussian 09, Revision D.01. Gaussian, Inc.: Wallingford CT, 2010.

(37) Becke, A. D.: Density-Functional Thermochemistry. III. The Role of Exact Exchange. *J. Chem. Phys.* **1993**, *98*, 5648-5652.

(38) Lee, C.; Yang, W.; Parr, R. G.: Development of the Colle-Salvetti Correlation-Energy Formula into a Functional of the Electron Density. *Phys. Rev. B* **1988**, *37*, 785-789.

(39) Küchle, W.; Dolg, M.; Stoll, H.; Preuss, H.: Energy-Adjusted Pseudopotentials for the Actinides. Parameter Sets and Test Calculations for Thorium and Thorium Monoxide. *J. Chem. Phys.* **1994**, *100*, 7535-7542.

(40) Cao, X.; Dolg, M.; Stoll, H.: Valence basis sets for relativistic energy-consistent small-core actinide pseudopotentials. *J. Chem. Phys.* **2003**, *118*, 487-496.

(41) Grimme, S.; Antony, J.; Ehrlich, S.; Krieg, H.: A consistent and accurate ab initio parameterization of density functional dispersion correction (DFT-D) for the 94 elements H-Pu. *J. Chem. Phys.* **2010**, *132*, 154104.

(42) Dunning Jr., T. H.: Gaussian basis sets for use in correlated molecular calculations. I. The atoms boron through neon and hydrogen. Ref to aug-cc-pVTZ. *J. Chem. Phys.* **1989**, *90*, 1007-1023.

(43) Reed, A. E.; Curtiss, L. A.; Weinhold, F.: Intermolecular interactions from a natural bond orbital, donor-acceptor viewpoint. *Chem. Rev.* **1988**, *88*, 899-926.

(44) Wiberg, K. B.: Application of the Pople-Santry-Segal CNDO method to the cyclopropylcarbinyl and cyclobutyl cation and to bicyclobutane. *Tetrahedron* **1968**, *24*, 1083-1096.

(45) Glendening, E. D.; Badenhoop, J. K.; Reed, A. E.; Carpenter, J. E.; Bohmann, J. A.; Morales, C. M.; Weinhold, F.: NBO 5.9. Theoretical Chemistry Institute, University of Wisconsin: Madison, US, 2011.

(46) Wheeler, O. W.; Carl, D. R.; Hofstetter, T. E.; Armentrout, P. B.: Hydration Enthalpies of Ba2+(H2O)(x), x=1-8: A Threshold Collision-Induced Dissociation and Computational Investigation. *Journal of Physical Chemistry A* **2015**, *119*, 3800-3815.

(47) Bush, M. F.; Saykally, R. J.; Williams, E. R.: Formation of hydrated triply charged metal ions from aqueous solutions using nanodrop mass spectrometry. *International Journal of Mass Spectrometry* **2006**, *253*, 256-262.

(48) Kretschmer, C. B.; Nowakowska, J.; Wiebe, R.: Solubility of Oxygen and Nitrogen in Organic Solvents from -25-Degrees-C to 50-Degrees-C. *Industrial and Engineering Chemistry* **1946**, *38*, 506-509.

(49) Ramos, C. I. V.; Pereira, P. M. R.; Santana-Marques, M. G.; De Paula, R.; Simoes, M. M. Q.; Neves, M. G. P. M. S.; Cavaleiro, J. A. S.: Imidazole and imidazolium porphyrins: gas-phase chemistry of multicharged ions. *Journal of Mass Spectrometry* **2014**, *49*, 371-379.

(50) Mallon, C.; Walshe, A.; Forster, R. J.; Keyes, T. E.; Baker, R. J.: Physical Characterization and Reactivity of the Uranyl Peroxide [UO2(eta(2)-O-2)(H2O)(2)]center dot 2H(2)O: Implications for Storage of Spent Nuclear Fuels. *Inorganic Chemistry* **2012**, *51*, 8509-8515.

(51) McGrail, B. T.; Pianowski, L. S.; Burns, P. C.: Photochemical Water Oxidation and Origin of Nonaqueous Uranyl Peroxide Complexes. *Journal of the American Chemical Society* **2014**, *136*, 4797-4800.

(52) Sullivan, J. C.; Gordon, S.; Cohen, D.; Mulac, W.; Schmidt, K. H.: Pulse-Radiolysis Studies of Uranium(VI), Neptunium(VI), Neptunium(V), and Plutonium(VI) in Aqueous Perchlorate Media. *Journal of Physical Chemistry* **1976**, *80*, 1684-1687.

(53) Dau, P. D.; Gibson, J. K.: Halide Abstraction from Halogenated Acetate Ligands by Actinyls: A Competition between Bond Breaking and Bond Making. *Journal of Physical Chemistry A* **2015**, *119*, 3218-3224.

(54) Bryantsev, V. S.; de Jong, W. A.; Cossel, K. C.; Diallo, M. S.; Goddard, W. A.; Groenewold, G. S.; Chien, W.; Van Stipdonk, M. J.: Two-electron three-centered bond in side-on (eta(2)) uranyl(V) superoxo complexes. *Journal of Physical Chemistry A* **2008**, *112*, 5777-5780.

(55) Leavitt, C. M.; Bryantsev, V. S.; de Jong, W. A.; Diallo, M. S.; Goddard, W. A.; Groenewold, G. S.; Van Stipdonk, M. J.: Addition of H2O and O-2 to Acetone and Dimethylsulfoxide Ligated Uranyl(V) Dioxocations. *Journal of Physical Chemistry A* **2009**, *113*, 2350-2358.

(56) Huheey, J. E.; Keiter, E. A.; Keiter, R. L.: *Inorganic Chemistry : Principles of Structure and Reactivity, 4th edition*; 4th ed.; HarperCollins: New York, USA, 1993.

(57) James, A. M.; Lord, M. P.: *Macmillan's Chemical and Physical Data*; Macmillan: London, UK, 1992.

(58) Qiu, J.; Ling, J.; Jouffret, L.; Thomas, R.; Szymanowski, J. E. S.; Burns, P. C.: Water-soluble multi-cage super tetrahedral uranyl peroxide phosphate clusters. *Chemical Science* **2014**, *5*, 303-310.

Table of Contents

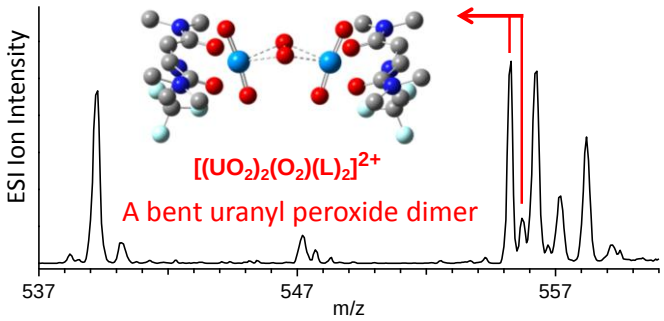

A gas-phase uranyl peroxide dimer coordinated by two polydentate electron-donor ligands was synthesized by electrospray ionization, and its reactivity was assessed. The dimer provides an elementary model to evaluate bonding and structures in bent uranyl peroxides, including nanospheres. Computations indicate that the uranyl peroxide structural motif is inherently planar with a dihedral U…O_2...U angle of 180°, but that minor energetic perturbations can induce substantial bending, to 145° in the synthesized gas-phase complex.